ACS OMEGA

pubs.acs.org/acsomega Volume 7, Issue 45 November 15, 2022

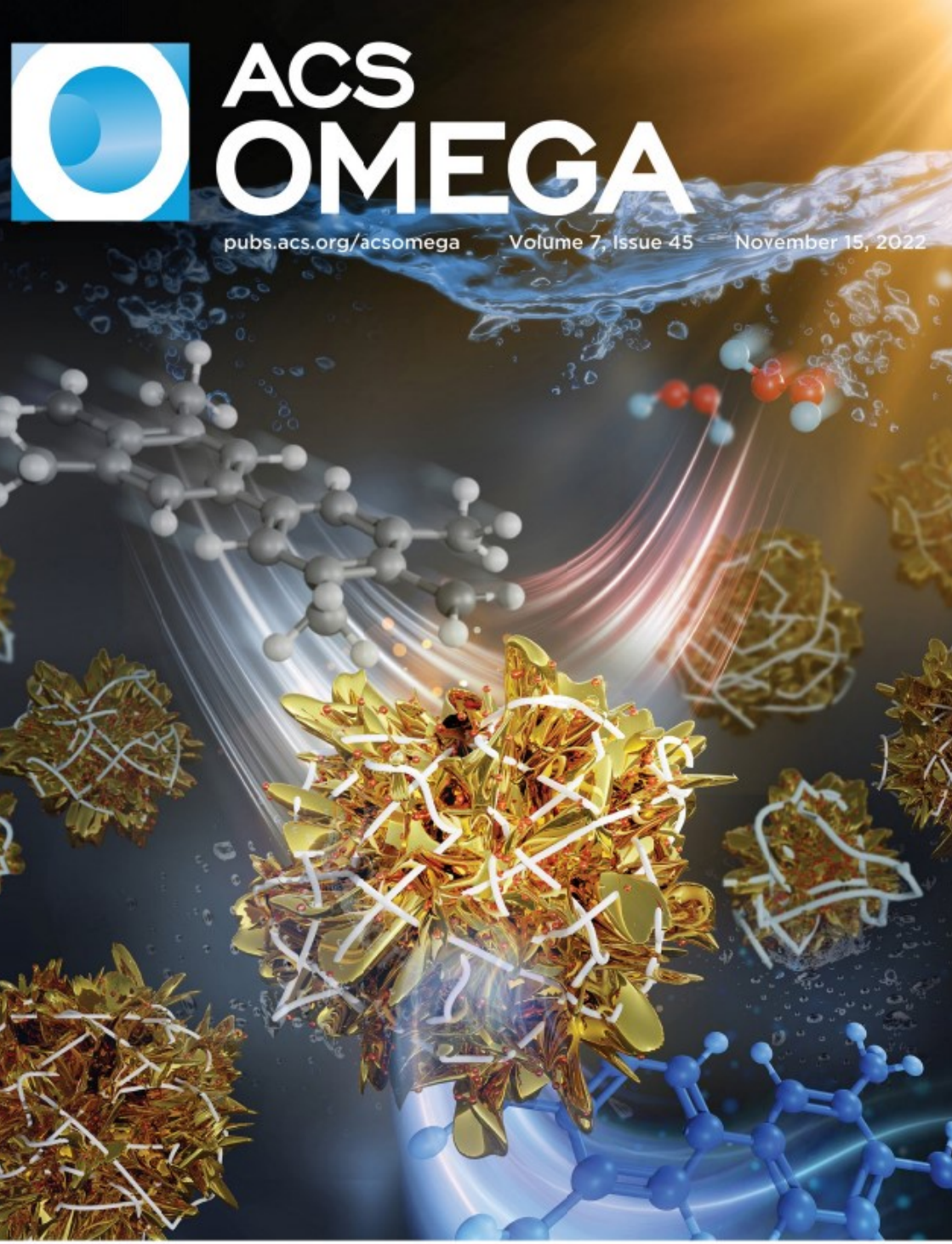

ACS Publications
Most Trusted. Most Cited. Most Read.

www.acs.org

ACS OMEGA

http://pubs.acs.org/journal/acsodf

Article

Multibranched Au–Ag–Pt Nanoparticle as a Nanozyme for the Colorimetric Assay of Hydrogen Peroxide and Glucose

Gyubok Lee, Changheon Kim, Dongwoo Kim, Changgi Hong, Taeyong Kim, Moongoo Lee, and Kangwon Lee*

Cite This: https://doi.org/10.1021/acsomega.2c04129

Read Online

ACCESS | Metrics & More | Article Recommendations | Supporting Information

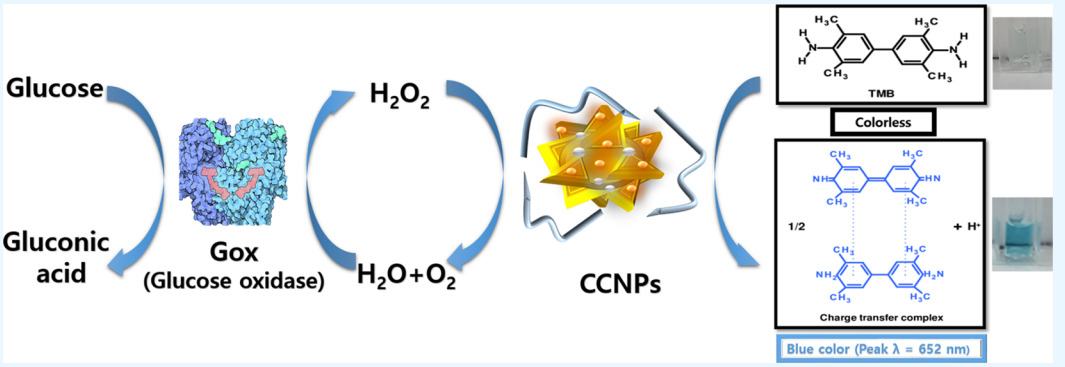

ABSTRACT: Many studies have recently produced artificial enzymes with metal nanoparticles (NPs) to overcome the limitations of natural enzymes, such as low stability, high cost, and storage problems. In particular, gold NPs exhibit peroxidase-like activity and are strongly influenced by external parameters, such as pH, temperature, size, shape, and functional layer, which change the enzyme activity. Here, chitosan-capped multibranched Au–Ag–Pt NPs (CCNPs) that mimic peroxidase were synthesized using various peroxidase-mimicking strategies. The results demonstrated that enzyme activity sequentially increased because of the multibranched Au–Ag NPs coated with Pt and chitosan. The enzyme activity of the particle was evaluated through the oxidation of 3,3′,5,5′-tetramethylbenzidine (TMB), which causes a color change into blue. This change was observable with the naked eye and could be used practically. The color change depended on the concentration of hydrogen peroxide (H_2O_2), and it was shown that the CCNPs could be applied to measure H_2O_2 with a limit of detection (LOD) of 0.054 mM. Furthermore, with glucose oxidase, the CCNPs can be used for glucose detection with an LOD of 0.289 mM. Also, the potential of the CCNP application in human serum was shown through the serum test. Thus, this study suggested the utilization of the multibranched Au–Ag–Pt NPs that mimic the peroxidase activity of natural enzymes and the possibility of application in various biological analyses.

Downloaded via SEOUL NATL UNIV on November 4, 2022 at 01:22:34 (UTC).
See https://pubs.acs.org/sharingguidelines for options on how to legitimately share published articles.

1. INTRODUCTION

Diabetes is a chronic disease caused by the resistance to insulin or inadequate insulin, causing complications in various body organs, such as the eyes, skin, liver, stomach, kidney, foot, blood vessels, nerves, and sexual organs.[1] Diabetes patients have a high incidence of cardiovascular (arteriosclerosis, stroke, angina, and myocardial infarction) and neurological complications (peripheral neuropathy, retinopathy, cataracts, and glaucoma). Diabetes can directly or indirectly affect many body organs; therefore, the failure to detect diabetes early can lead to the rapid deterioration of health owing to complications.

Various methods have been developed to measure blood sugar or glucose contents in body fluids for the early diagnosis of diabetes. In these methods, colorimetric detection is inexpensive and highly versatile. Conventionally, for colorimetric detection, hydrogen peroxide (H_2O_2) is generated using glucose and glucose oxidase, and the generated H_2O_2 is combined with peroxidase to oxidize the chromogenic agent.[2] However, the peroxidase used in this process is a natural enzyme derived from living organisms. Natural enzymes are mainly protein-based compounds, and enzyme activity is greatly affected by the changes in temperature, pH, and salt concentration.[3] In a study that confirmed the enzymatic activity of peroxidase, the enzyme activity decreased by 30% when the temperature was near the body temperature. Outside a pH of 7, the enzyme activity sharply dropped, and the

Received: July 1, 2022
Accepted: October 21, 2022
Published: November 2, 2022

© 2022 The Authors. Published by American Chemical Society

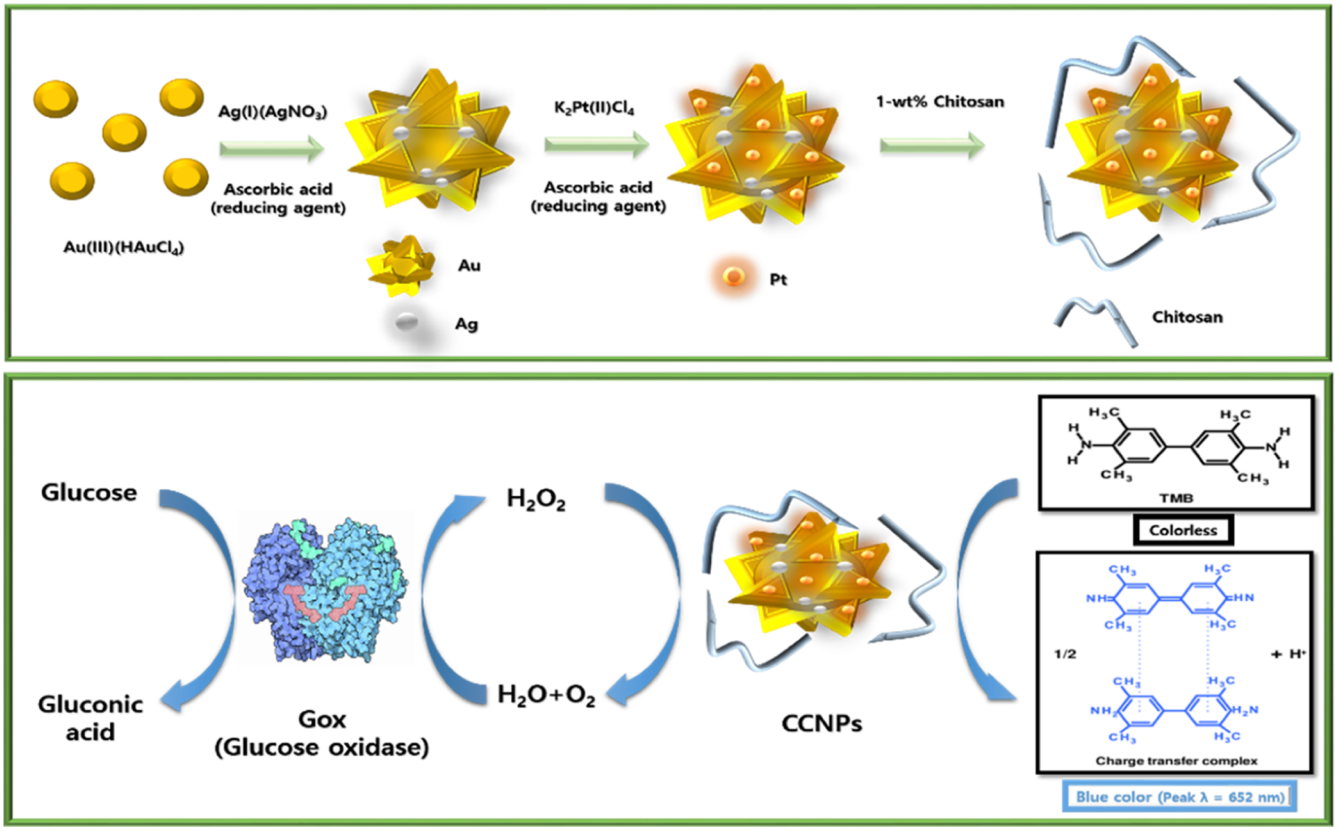

Figure 1. Illustration of the reaction cascade for glucose detection using CCNPs.

enzyme activity sharply dropped even with a change in the salt concentration.

To replace protein-based enzymes extracted from nature, previous studies have been conducted to replace the role of enzymes based on nonprotein-based nanoparticles (NPs), including noble metals (Au,[4] Ag,[5] Pt,[6] and Pd[7]), transition metal oxides (Fe_3O_4,[8] CuS,[9] Fe_3S_4,[10] and CuZnO[11]), and carbon nanomaterials (single-walled carbon nanotube, multi-walled carbon nanotube, and graphene).[12] These are called nanozymes.[13] Nanozymes are created using many different enzyme mimicking strategies. The usage of Au NPs is one of them. Au NPs have been used to mimic various enzymes, such as oxidase,[14] superoxide dismutase (SOD),[15] catalase,[16] peroxidase,[17] and glucose oxidase.[18] Moreover, Au NPs possess the advantage of maximizing the surface-interface resolution owing to the plasmon effect through surface modification.[19] This indicates that the specific chemical reaction of the material to be analyzed on the surface of the Au NP can be maximized.[20,21] Recently, it was discovered that the morphology of Au NPs can be changed to maximize the enzyme function.[22,23] To increase the surface chemistry efficiency of NPs, a study established a method of increasing the surface area. Methods for manufacturing NPs in various forms/shapes, such as the porous structure, star shape, and rod shape, have been developed.[24] Especially, it was found that in the process of growing Au NPs, Ag NPs were reduced to the surface, thereby inhibiting the growth of the Au NPs and exhibiting a star-shaped morphology.[25] According to the previous research, the star-shaped NPs showed a 60% increase in surface area to volume compared to the spherical NPs.[26] In addition, the enzymatic performance of spherical and star-shaped NPs was directly compared. The activity of the star-shaped NPs was higher than that of the spherical gold NPs.[27]

In addition, studies have been conducted to change the composition of the surface chemistry to increase the catalytic activity. Au NPs were manufactured in the form of nanorods[28] and urchins[29] by covering Au NPs with Pt, and it was observed that the higher the Pt fraction on the particle surface, the higher the catalytic activity.[30] Chitosan is also used to enhance the peroxidase activity. Chitosan is a polysaccharide derived from chitin and is specifically polycational and chelating using amino and hydroxyl groups.[31] It is known that the polycation of chitosan can mimic the peroxidase enzyme because of its surface charge.[32] In addition, metal ions could be uniformly distributed around chitosan because of chelation, thereby increasing the stability of the generated NPs.[33,34]

Here, we produced chitosan-capped multibranched Au−Ag−Pt NPs (CCNPs) by applying the aforementioned peroxidase-mimicking strategies (Figure 1). To date, no study has applied strategies, such as particle shape change, surface modification through Pt coating, and charge change and stability enhancement through polymer coating at once to develop nanozymes to mimic peroxidase. Moreover, by merely mixing the ingredients, CCNPs can be produced in situ in about an hour at room temperature. The surface evaluation was performed through scanning electron microscopy (SEM). Afterward, enzyme activity was measured using an ultraviolet−visible (UV−vis) spectrophotometer to quantitatively analyze its ability to replace natural horseradish peroxidase (HRP). We applied it to glucose measurements. This suggested a great potential for the peroxidase replacement of CCNPs for biodetection.

https://doi.org/10.1021/acsomega.2c04129
ACS Omega XXXX, XXX, XXX−XXX

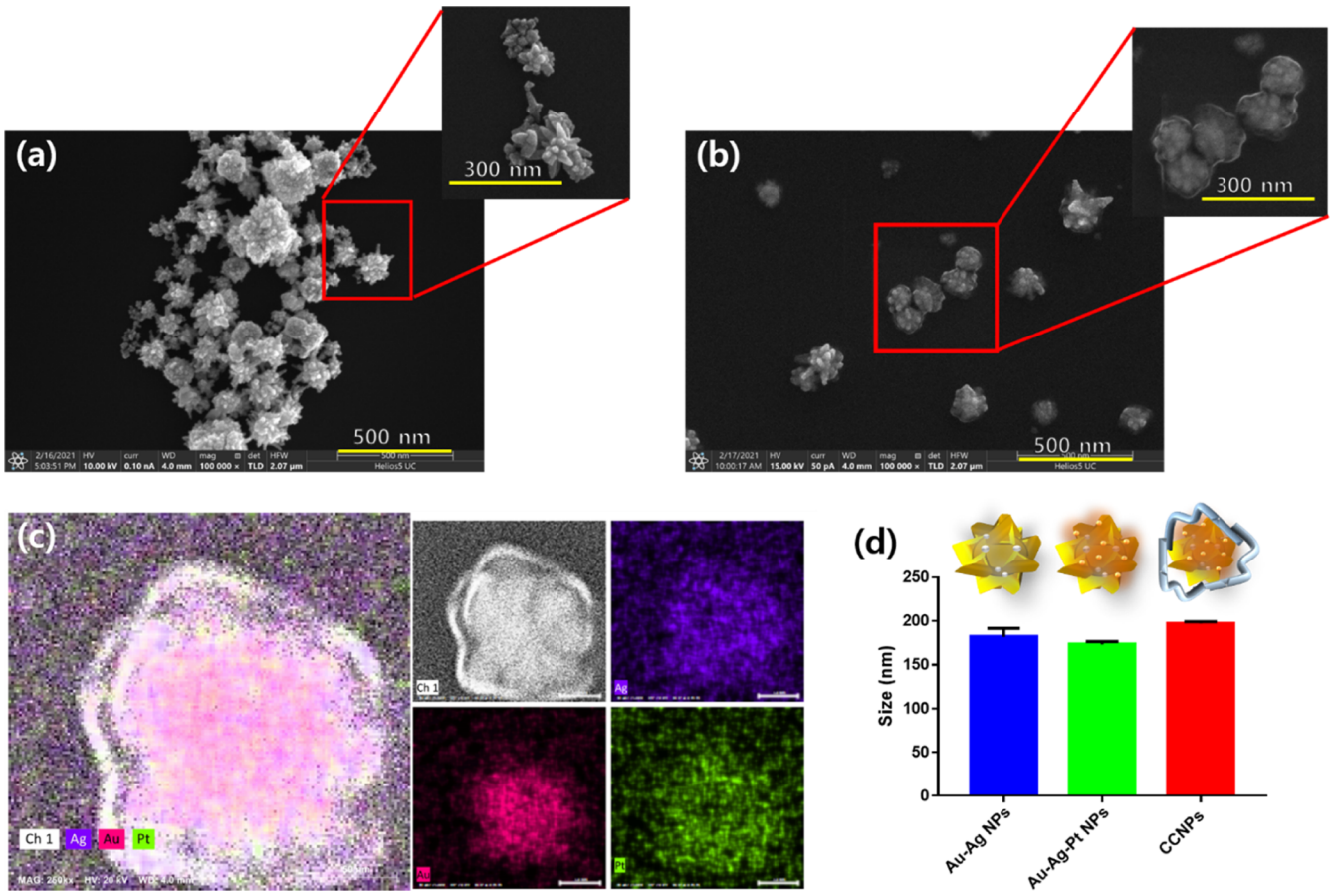

Figure 2. SEM images of (a) multibranched Au−Ag−Pt NPs and (b) CCNPs. (c) SEM-EDS analysis of Ag, Au, and Pt in CCNPs. (d) DLS data of Au−Ag NPs, Au−Ag−Pt NPs, and CCNPs.

2. RESULTS AND DISCUSSION

2.1. Characterization of CCNPs. The multibranched Au−Ag−Pt NPs and CCNPs were characterized by SEM. The multibranched Au−Ag−Pt NPs were spherical with multiple branches, and their sizes were in a range of 150−200 nm (Figure 2a). Therefore, the formation of multibranched NPs with an increased specific surface area was confirmed. It was observed that the CCNPs were surrounded by a thin film produced by chitosan and there was no significant difference in size with the bare Au−Ag−Pt NPs (Figure 2b). The CCNPs were characterized by TEM (Figure S1). Figure S1 shows that the multibranched forms were observed at a high magnification.

The SEM-EDS mapping shows the distribution of Au, Ag, and Pt in the CCNPs (Figure 2c). Au, Ag, and Pt are indicated in red, purple, and green, respectively. The concentration of red dots is high at the core; therefore, it was considered that Au was distributed in the core of the NPs. Importantly, Ag was scattered on the Au surface. According to Cheng et al., adding Ag to the Au NPs changed the morphology of the NPs. As the Ag concentration increased, the NPs became multibranched and irregularly quasi-spherical. Au ions have a higher reduction potential than Ag ions; therefore, on the surface of the reduced Au NPs, the Ag ions were first reduced and served as an active surface for further growth.[35] Accordingly, the multibranched morphology with a larger specific surface area than those of the Au NPs was created, thereby exhibiting a stronger enzyme activity. In addition, Pt was scattered over the CCNPs. The distributions of the Au, Ag, and Pt elements in the CCNPs were determined by quantitative analysis of the each element intensity in the SEM-EDS data to be 44.24, 27.66, and 28.10%, respectively. As a result of XPS data analysis, gold and silver were not observed on the surface, indicating that the star-shaped gold NPs, which are the core of the particles, are not active sites. However, since the elements of Pt and chitosan were observed in the XPS data, it can be expected that Pt and chitosan, which have intrinsic peroxidase mimic ability, are active sites (Figure S2).

The particle sizes of the Au−Ag NPs, Au−Ag−Pt NPs, and CCNPs were measured by DLS to be 181.9, 178.3, and 197.2 nm, respectively (Figure 2d). There was a minimal change in the particle size because of the Pt coating, and the particle size increased by approximately 15 nm after the chitosan coating. Furthermore, the absorption bands from the Au−Ag−Pt NPs and CCNPs were recorded by Fourier transform infrared (FT-IR) spectroscopy. Then, the IR spectrum of the Au−Ag−Pt NPs and CCNPs was compared (Figure S3). As shown in the IR spectrum of the CCNPs, the bands at 1215 and 1550 cm^{-1} showed the presence of C−O and N−H peaks from chitosan, respectively. As shown in the IR spectrum of the Au−Ag−Pt NPs, the aforementioned peaks were not observed. Thus, it was confirmed that the CCNPs were coated with chitosan.

2.2. Peroxidase-like Activity of CCNPs. We confirmed that the CCNPs exhibited peroxidase-like activity (Figure 3a). The CCNPs decomposed H_2O_2 and oxidized TMB. The UV−vis spectra of the oxidized TMB (ox-TMB) exhibited a characteristic peak at 652 nm. Prior to verifying the peroxidase

https://doi.org/10.1021/acsomega.2c04129
ACS Omega XXXX, XXX, XXX−XXX

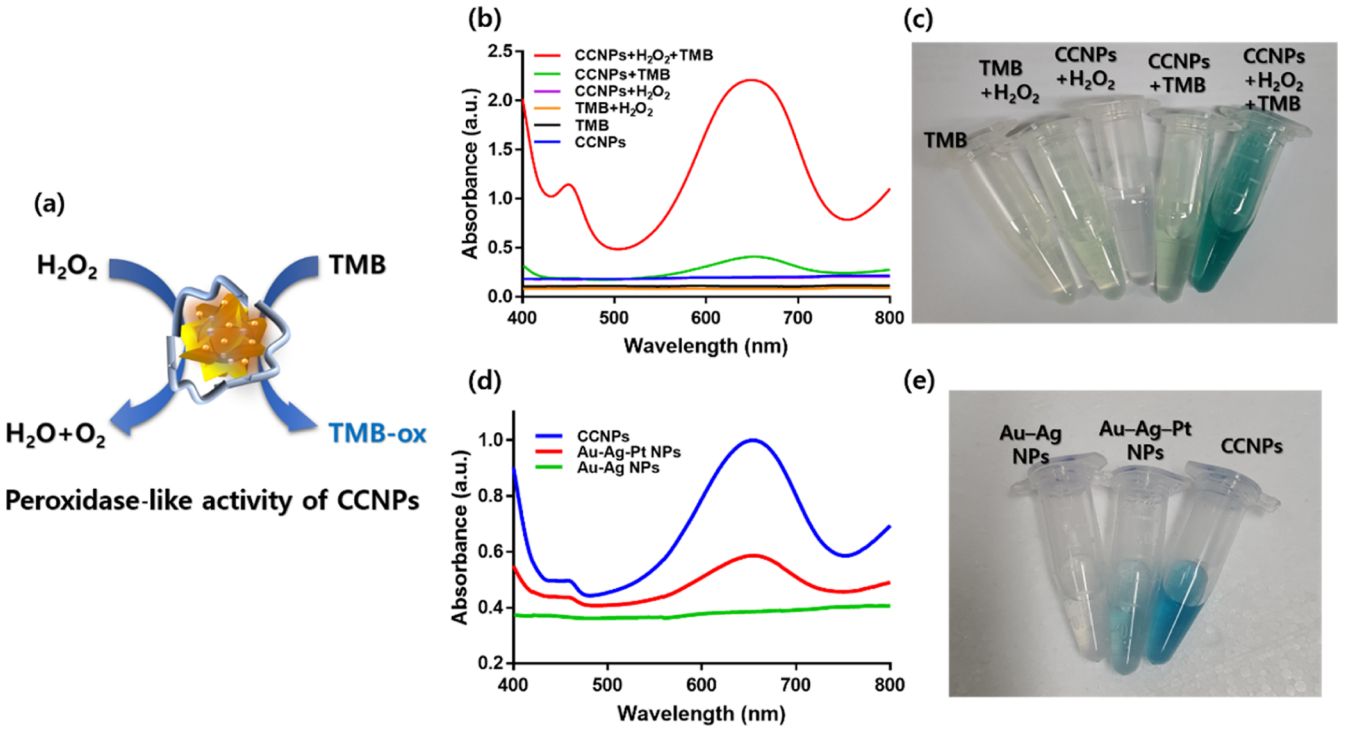

Figure 3. (a) Schematic illustration of peroxidase-like activity of CCNPs. (b) UV−vis absorbance spectra of CCNPs, TMB, TMB + H_2O_2, CCNPs + H_2O_2, CCNPs + TMB, and CCNPs + H_2O_2 + TMB in peroxidase-like activity test. (c) Images corresponding to the spectra shown in Figure 3b. (d) UV−vis absorbance spectra of Au−Ag NPs, Au−Ag−Pt NPs, and CCNPs in the peroxidase-like activity test. (e) Images corresponding to the spectra shown in Figure 3d.

activity of the CCNPs, we conducted various optimization experiments. First, the change in absorbance at 652 nm according to the Pt concentration was compared (Figure S4). As Pt was added, the absorbance rapidly increased even at low concentrations. The volume of 10 mM Pt showed the greatest change in absorbance when 50 μL was added, followed by a decrease. Thus, we set the optimal Pt concentration. The change in absorbance by the CCNPs according to temperature and pH was then measured. The changes in absorbance at 652 nm were measured in the temperature range of 20−80 °C (Figure S5a). The absorbance was the highest at 20 °C, and there was no significant change in the absorbance up to 60 °C despite the increase in temperature. However, a sharp change in absorbance occurred above 60 °C. Therefore, it was confirmed that the normal activity temperature of CCNPs ranged between 4 and 60 °C. The absorbance at 652 nm according to the pH range of 1−10 was measured and plotted through normalization (Figure S5b). The highest change in absorbance was observed at a pH between 4 and 8. The change in absorbance remarkably decreased at a pH of 4 or less and 8 or more. Therefore, it was confirmed that the normal activity pH of CCNPs was between 4 and 8. The temperature of most body fluids is approximately 37 °C, and the pH of most body fluids is around 7.4. Thus, it was confirmed acceptable for practical use as a biosensor. The absorbance at 652 nm with time was recorded (Figure S6). Initially, the absorbance gradually increased with time, but after 5 min, it was saturated at a constant value. In addition, the absorbance tended to slightly decrease over time. Therefore, 5 min was set as the saturation time of the reaction, and the experiment was conducted.

After optimizing various conditions such as the pH, temperature, and time, the peroxidase-like activity of CCNP was verified. Before verification, the spectra of Au−Ag NPs, Au−Ag−Pt NPs, and CCNPs itself were measured (Figure S7). Figure 3b shows the spectra of the five conditions by UV−vis spectroscopy. Dissimilar to the other conditions, strong absorption bands were observed around 652 nm only when CCNPs, H_2O_2, and TMB were present. TMB could be oxidized because the CCNPs exhibited peroxidase-like activity that decomposed H_2O_2. Figure 3c shows the image of each experimental condition. Dissimilar to the remaining experimental conditions with transparent or light yellow or green light, strong color light was observed in the experiment in which CCNPs, H_2O_2, and TMB were reacted.

As previously mentioned, we improved the peroxidase-like activity of the metal NPs by adding Pt to Au−Ag NPs. Furthermore, they were coated with chitosan to prevent the aggregation of the Au−Ag−Pt NPs and increase the catalytic activity. To confirm the effectiveness of these strategies, the peroxidase-like activities of the Au−Ag NPs, Au−Ag−Pt NPs, and CCNPs were measured. Figure 3d shows the UV−vis spectra of the peroxidase-like activities of the three aforementioned NPs. The Au−Ag NPs did not exhibit a significant peak around 650 nm, but the Au−Ag−Pt NPs exhibited an absorbance around 0.5. However, this absorbance was so weak that it was incomparable to that of the CCNPs. The CCNPs exhibited an absorbance around 1.0 and showed the strongest peroxidase-like activity. Figure 3e shows the results of the colorimetric observation. The Au−Ag NPs appeared practically transparent, and the Au−Ag−Pt NPs had a pale-blue light, while the CCNPs had the strongest blue light. Thus, it was confirmed that the enzyme activity gradually increased as Pt and chitosan were added.

2.3. Sensitivity of CCNPs against H_2O_2 and TMB. To determine the extent of the peroxidase-like activity of the

https://doi.org/10.1021/acsomega.2c04129
ACS Omega XXXX, XXX, XXX−XXX

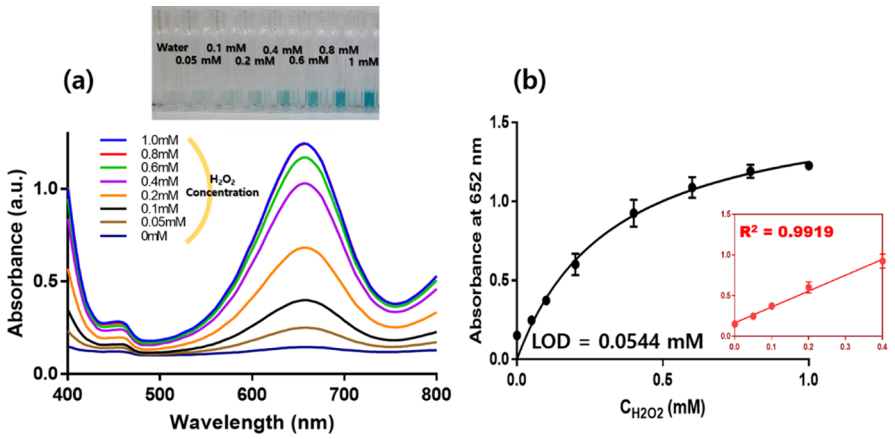

Figure 4. Sensitivity of CCNPs at different H_2O_2 concentrations. (a) UV−vis absorption spectra of the sensing platform with increase in the concentration of H_2O_2 (0.05−1.00 mM). Inset shows the images of the colorimetric detection of H_2O_2. (b) Correlation between the content of H_2O_2 and the absorbance at 652 nm. Inset plot shows the reaction of the initial concentration.

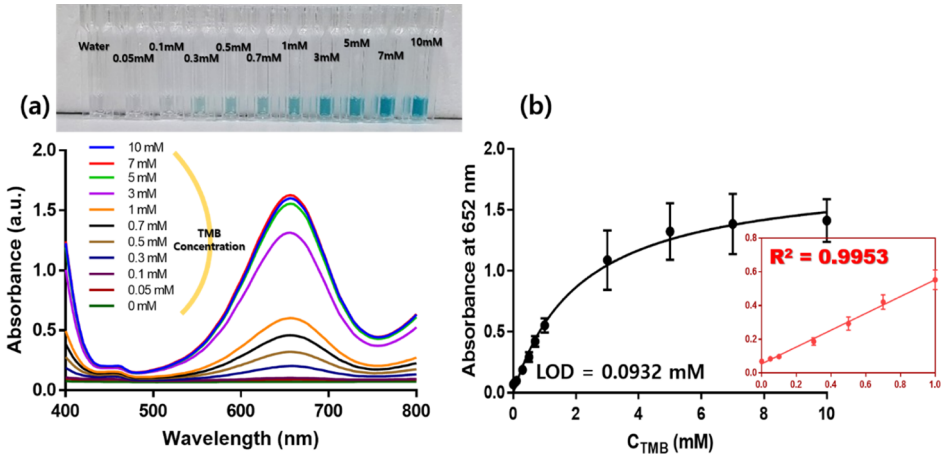

Figure 5. Sensitivity of CCNPs at different TMB concentrations. (a) UV−vis absorption spectra of the sensing platform with an increase in the concentration of TMB (0.05−10.0 mM). Inset shows the images for various concentrations of TMB. (b) Correlation between the content of TMB and the absorbance at 652 nm. Inset plot shows the reaction of the initial concentration.

CCNPs, we measured the absorbance at different H_2O_2 concentrations. The H_2O_2 concentration was sequentially adjusted from 0 to 1 mM. When observed with the naked eye, from 0 mM, the higher the concentration, the darker the blue light. As shown in each UV−vis spectra, the absorbance increased as the H_2O_2 concentration increased (Figure 4a). Each maximum absorbance wavelength was 652 nm (a characteristic peak of ox-TMB). Figure 4b shows the correlation between the absorbance and the H_2O_2 concentration. When the H_2O_2 concentration was low, the absorbance linearly increased as the substrate concentration increased. As the substrate concentration increased, it did not appear linearly because the enzymes were saturated. This indicated that H_2O_2 was detected in proportion to the degree to which the solution had blue light. At this time, the R-square value was 0.9919. The limit of detection (LOD) value was obtained by (standard error/slope) × 3.3. The standard error refers to the amount of error of the predicted absorbance value for the H_2O_2 concentration. The LOD for H_2O_2 was calculated to be 0.0544 mM.

We then measured the absorbance at different TMB concentrations. The TMB concentrations were sequentially adjusted from 0 to 10 mM. When observed with the naked eye, from 0 mM, the higher the concentration, the darker the blue light. As the TMB concentration increased, the UV−vis absorbance value at 652 nm (the maximum absorbance wavelength) also increased (Figure 5a). The association between the absorbance value and TMB concentration is depicted in Figure 5b. When the TMB concentration was low, the absorbance linearly increased as the substrate concentration increased. This indicated that the TMB was detected in proportion to the degree to which the solution had blue light. The R-square value was 0.9953. The LOD of TMB was calculated similarly to that of H_2O_2 to be 0.0932 mM.

2.4. Kinetic Analysis of CCNPs. Michaelis−Menten kinetics is one of the most well-known models of enzyme reaction kinetics in biochemistry. Through this kinetics, the initial reaction rate at different substrate concentrations can be calculated. The reaction rate was expressed by eq 1.

$$V = \frac{V_{max}[s]}{[s] + K_m} \quad (1)$$

$$A = \varepsilon cl \quad (2)$$

$$\frac{1}{V} = \frac{K_m}{V_{max}[s]} + \frac{1}{V_{max}} \quad (3)$$

https://doi.org/10.1021/acsomega.2c04129
ACS Omega XXXX, XXX, XXX−XXX

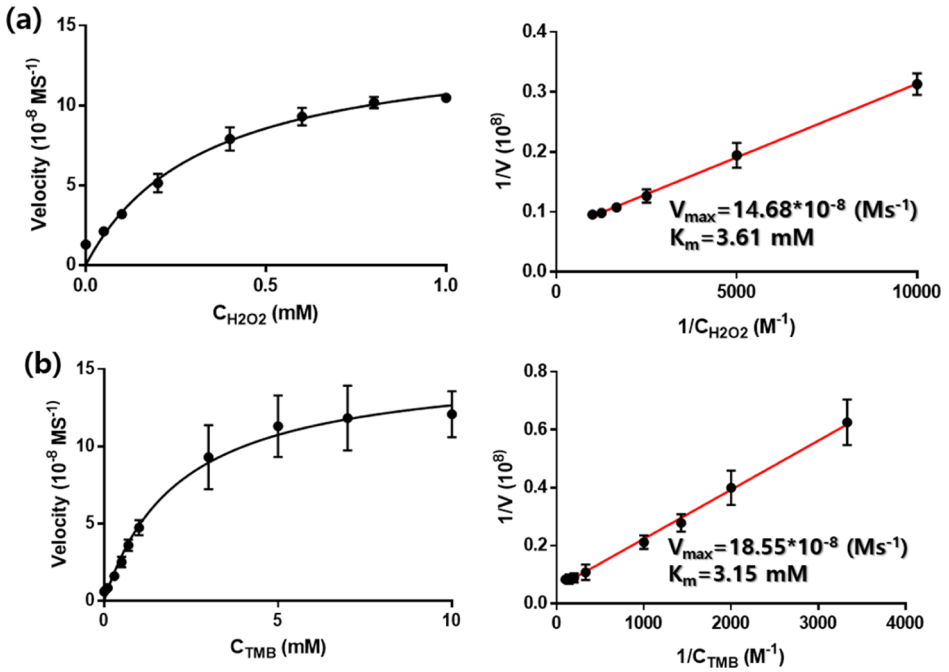

Figure 6. Reaction rate of CCNPs at different H_2O_2 and TMB concentrations. (a) Steady-state kinetic assay of CCNPs at varied H_2O_2 concentrations. (b) Steady-state kinetic assay of CCNPs at varied TMB concentrations.

The smaller the K_m value, which is the Michaelis constant, and the larger the V_{max} value, which is the maximum reaction rate, the higher the reaction rate. We used Beer−Lambert's law equation to calculate the concentration from the absorbance and molar extinction coefficient using eq 2. The molar extinction coefficient of ox-TMB is 39000 M^{-1} cm^{-1},[36] and the path length of the cuvette is 1 cm. Therefore, the molar concentration was obtained by substituting the absorbance at 652 nm into this equation. The reaction rate was obtained by dividing the change in the molar concentration by the reaction time. When the conditions of the other reagents were the same, the reaction rate according to the H_2O_2 concentration changed (Figure 6a). At this time, when the graph is illustrated by taking the reciprocal of each variable, the first-order function was obtained as eq 3.

K_m and V_{max} were obtained using the slope and y-intercept of the straight line, Lineweaver−Burk plot. The V_{max} and K_m values were 14.68 × 10^{-8} M/s and 3.61 mM, respectively. This was a better value than those of PT50-PEI or Au NPs, which are reported nanozymes, and HRP, which was used as a conventional natural enzyme (Table 1). In addition, the reaction rate with time was compared by fixing the H_2O_2 concentration and varying the TMB concentration (Figure 6b). In that case, the V_{max} and K_m values were 18.55 × 10^{-8} M/s and 3.15 mM, respectively.

Table 1. Comparison of Different Enzymes with K_m and V_{max} Values[37−42]

enzyme	K_m (mM)	V_{max}	refs
CCNPs	3.61	14.68	this work
HRP	3.70	8.71	37
CNZ	25	0.038	38
Pt50-PEI	43.60	8.5	39
PtNPs/GO	221.4	12.45	40
Fe_3O_4 MNPs	154	9.78	41
Au NPs	33	6.1	42

2.5. Glucose Detection. We confirmed the detection sensitivity of CCNPs for glucose. To achieve the ultimate goal of colorimetric glucose detection, CCNPs must accurately and sensitively detect low glucose concentrations. The inset of Figure 7a is an image of the cuvettes reacted with CCNPs and TMB by varying the glucose concentration from 0 to 10 mM. The higher the glucose concentration, the darker the blue light. Moreover, we recorded the UV−vis spectra by changing the glucose concentration from 0 to 10 mM (Figure 7a). Using a UV−vis spectrophotometer, the absorbance was shown to rise as the glucose concentration increased. Figure 7b shows the absorbance at 652 nm according to the glucose concentration. When the glucose concentration was low, the absorbance linearly increased as the glucose concentration increased. At this time, the *R*-square value was 0.9959. The LOD of glucose was 0.2896 mM. This indicated that glucose was detected in proportion to the degree to which the solution had blue light.

2.6. Selectivity Test and Serum Test. The sensitivity of the glucose detection was evaluated with maltose, galactose, sucrose, and lactose as controls. The concentrations of the sugars used were 10 mM. Figure 8a shows that the absorbance of the control group was considerably lower than that of glucose. Therefore, this detection method showed a high glucose selectivity due to the selective oxidation of glucose by glucose oxidase. Next, the serum application test was conducted to see if the CCNPs could be applied to human serum. UV−vis spectra were recorded by adding the glucose concentration from 0 to 1 mM to a 10-fold diluted serum (Figure 8b). Using a UV−vis spectrophotometer, the absorbance was shown to rise as the glucose increased. Figure 8c shows glucose concentration versus 652 nm absorbance with an *R*-square value of 0.941 and an LOD of 0.3778 mM. Therefore, CCNPs showed the potential to be applied to glucose measurement in human serum.

https://doi.org/10.1021/acsomega.2c04129
ACS Omega XXXX, XXX, XXX−XXX

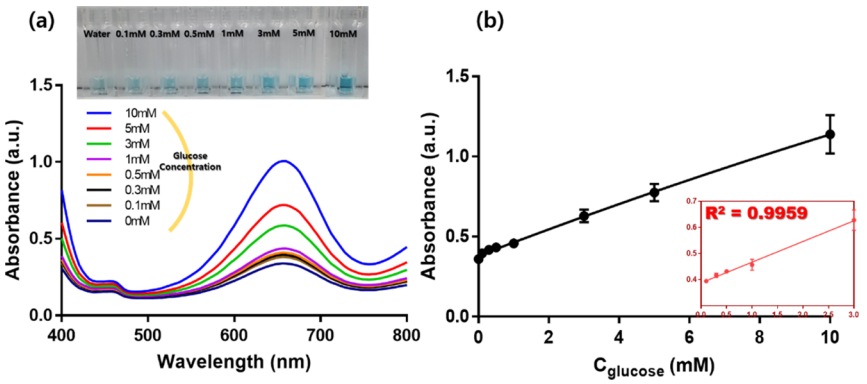

Figure 7. Glucose detection of CCNPs at different concentrations. (a) UV−vis absorption spectra of the sensing platform at different concentrations of glucose (0.1−10 mM). Inset shows theimages for various concentrations of glucose. (b) Correlation between the content of glucose and the absorbance at 652 nm. Inset plot shows the reaction of the initial concentration.

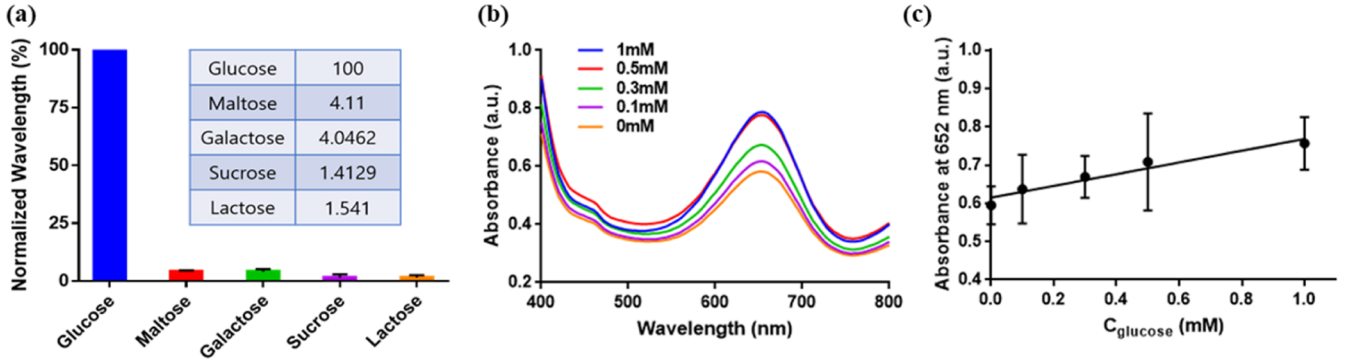

Figure 8. (a) Selectivity analysis of CCNPs for glucose detection. The normalization result of the 652nm wavelength value according to 10 mM glucose, maltose, galactose, sucrose, and lactose. The inset table is a comparison result of the normalized intensity. (b) UV−vis absorption spectra of the sensing platform at different glucose concentrations (0.1−1 mM) in a 10-fold diluted serum. (c) Correlation between the content of glucose in a 10-fold diluted serum and the absorbance at 652 nm.

3. CONCLUSIONS

Here, we observed the peroxidase-like activity of CCNPs. We increased the catalytic activity by adding Pt to the Au−Ag NPs, which were known to exhibit better peroxidase-like activity, and coating them with chitosan. The characterization of the NPs was completed by SEM, SEM-EDS, TEM, XPS, FTIR, and DLS. The peroxidase-mimicking enzymes decomposed H_2O_2 and oxidized TMB, which emits blue light. Here, CCNPs (artificial enzymes), H_2O_2, and TMB were reacted. We observed a strong peak around 652 nm using a UV−vis spectrophotometer. Moreover, the higher the concentration of H_2O_2 or TMB, the higher the catalytic activity. The LOD values for H_2O_2 or TMB were 0.0504 and 0.0932 mM, respectively. Using Michaelis−Menten kinetics, the V_{max} and K_m values were 14.68×10^{-8} M/s and 3.61 mM, respectively. This was a better value than those of a reported nanozyme or natural enzyme. Finally, after measuring the catalytic activity of CCNPs at different glucose concentrations, it was observed that the absorbance proportionally increased as the glucose concentration increased. Therefore, it is expected that the CCNPs can be effectively used for the easy and early diagnosis of diabetes in the developing countries.

4. MATERIALS AND METHODS

4.1. Chemicals and Reagents. Gold(III) chloride hydrate ($HAuCl_4 \cdot H_2O$), silver nitrate ($AgNO_3$), potassium tetrachloroplatinate(II) (K_2PtCl_4), glucose oxidase from *Aspergillus niger* (GOx), ascorbic acid, ethanol, acetic acid, human serum, and HRP were purchased from Sigma-Aldrich (St. Louis, USA). In addition, 3,3′,5,5′-tetramethylbenzidine (TMB) and glucose were purchased from TCI (Tokyo, Japan). Chitosan, maltose monohydrate, fructose, lactose monohydrate, galactose, and H_2O_2 were obtained from Samchun Chemicals (Seoul, Korea). All chemicals and reagents were of analytical grade.

4.2. Instruments. SEM and energy-dispersive X-ray spectroscopy (EDS) mapping images were obtained using a focused ion beam scanning electron microscope (Helios 5 UC, FEI). Transmission electron microscopy (TEM) images were captured using a high-resolution transmission electron microscope (JEM-3010, JEOL). Dynamic light scattering (DLS) was measured using a Zetasizer (Zetasizer Nano ZS, Malvern Instruments). UV−vis spectra were recorded using UV−vis spectroscopy (Lambda 25 UV−vis spectroscopy, PerkinElmer) and a microplate reader (Synergy H1, BioTek).

4.3. Preparation of CCNPs. In order to synthesize the Au−Ag NPs, 20 μL of the 10 mM $HAuCl_4$ aqueous solution and 1000 μL of DI water were mixed into the vial and vortexed. Afterward, 5 μL of a 10 mM $AgNO_3$ aqueous solution was added, followed by 4 μL of 100 mM ascorbic acid. The mixture was then vortexed after 50 μL of 10 mM K_2PtCl_4 was added. A 1 wt % chitosan solution was then prepared using ethanol as a solvent. Aqueous NP solution that had already been made and the chitosan solution were combined 1:1 and agitated for 24 h. The collected NP solution was washed with

https://doi.org/10.1021/acsomega.2c04129
ACS Omega XXXX, XXX, XXX−XXX

DI water three times and stored at room temperature for further use.

4.4. Characterization of CCNPs. SEM and TEM were used to observe the CCNPs' morphology and size. To examine the distribution of different elements in CCNPs, SEM-EDS was used. The sizes of the Au−Ag NPs, Au−Ag−Pt NPs, and CCNPs were compared through DLS. The absorbance of CCNPs was measured using UV−vis spectroscopy to confirm if it exhibited peroxidase-like activity.

4.5. Peroxidase-like Activity of CCNPs. To observe the decomposition of H_2O_2 using CCNPs, we set five conditions. Each vial contained or did not contain CCNPs, H_2O_2 (10 mM), or TMB (10 mM). The five conditions were as follows: DI water (800 μL) and TMB (100 μL); DI water (400 μL), H_2O_2 (400 μL), and TMB (100 μL); CCNP solution (400 μL), H_2O_2 (400 μL), and DI water (100 μL); CCNP solution (400 μL), TMB (100 μL), and DI water (400 μL); and CCNP solution (400 μL), H_2O_2 (400 μL), and TMB (100 μL). The maximum absorbance wavelength and value of absorbance were measured using a UV−vis spectrophotometer for each condition.

4.6. Comparison of Peroxidase-like Activity for Au−Ag NPs, Au−Ag−Pt NPs, and CCNPs. To compare the peroxidase-like activity of the Au−Ag NPs, Au−Ag−Pt NPs, and CCNPs, 1 mM H_2O_2 (500 μL) and 10 mM TMB (100 μL) were reacted with 1000 μL of each aqueous NP solution. Each was measured using a UV−vis spectrophotometer.

4.7. Peroxidase-like Activity of CCNPs for Temperature, pH, and Incubation Time. In the temperature experiment, 1 mM TMB and H_2O_2 were reacted for 5 min with the CCNP solution at different temperatures from 4 to 80 °C. Thereafter, the absorbance at 652 nm at different temperatures was recorded. In the pH experiment, 1 mM TMB and H_2O_2 were reacted for 5 min with the CCNP solution adding buffers of different pH from pH 1 to pH 10. Thereafter, the absorbance at 652 nm at different pH was recorded. In the incubation time experiment, 1 mM TMB and H_2O_2 were reacted for 5 min with the CCNP solution at different time intervals from 0 to 10 min. Thereafter, the absorbance at 652 nm at different time intervals was recorded.

4.8. Sensitivity of CCNPs against H_2O_2 and TMB. The H_2O_2 concentration was increased from 0 to 0.05, 0.1, 0.2, 0.4, 0.6, 0.8, and 1 mM and reacted with the CCNP solution (100 μL) and 1 mM TMB (100 μL). The mixtures were examined using a UV−vis spectrophotometer after 5 min of incubation at 37 °C. Thereafter, the absorbance at 652 nm at different concentrations of H_2O_2 was recorded.

Similarly, the TMB concentration was increased from 0 to 0.05, 0.1, 0.3, 0.5, 0.7, 1, 3, 5, 7, and 10 mM, reacting with the CCNP solution (100 μL) and 0.2 mM H_2O_2 (100 μL). The mixtures were incubated for 5 min at 37 °C. Thereafter, the absorbance at 652 nm at different concentrations of TMB was recorded.

4.9. Glucose Detection. The glucose concentration was increased from 0 to 0.1, 0.3, 0.5, 1, 3, 5, and 10 mM, and the glucose was reacted with glucose oxidase at 50 °C for 10 min. The mixtures were reacted with the CCNP solution (100 μL) and 10 mM TMB (100 μL). Then, the mixtures were examined using a UV−vis spectrophotometer after 5 min of incubation at 37 °C. Thereafter, the absorbance at 652 nm at different glucose concentrations was recorded.

4.10. Selectivity of CCNPs. 10 mM glucose, maltose, galactose, sucrose, and lactose were reacted with glucose oxidase at 50 °C for 10 min. The mixtures were incubated with 100 μL each of the 10 mM TMB solution and the CCNP solution for 5 min at 37 °C. Thereafter, the absorbance at 652 nm at different sugars was recorded. The absorbance at 652nm was normalized to the absorbance of the mixture to which TMB, glucose oxidase, and CCNP were added. The minimum value was set to a wavelength of 652 nm in the control experiment, and the maximum value was set to a wavelength value of 652 nm in the 10 mM glucose reaction experiment for normalization.

4.11. Serum Test of CCNPs. Human serum for the experiment was diluted 10-fold. The glucose concentration in a 10-fold diluted serum was increased from 0 to 0.1, 0.3, 0.5, and 1 mM, and the glucose was reacted with glucose oxidase at 50 °C for 10 min. The mixtures were reacted with the CCNP solution (100 μL) and 10 mM TMB (100 μL). Then, the mixtures were examined using a UV−vis spectrophotometer after 5 min of incubation at 37 °C. Thereafter, the absorbance at 652 nm at different glucose concentrations was recorded. All the above experiments were repeated at least three times.

■ ASSOCIATED CONTENT

Supporting Information

The Supporting Information is available free of charge at https://pubs.acs.org/doi/10.1021/acsomega.2c04129.

TEM images, FTIR spectra, XPS spectra, and UV−vis spectra for all compounds (PDF)

■ AUTHOR INFORMATION

Corresponding Author

Kangwon Lee − *Department of Applied Bioengineering, Graduate School of Convergence Science and Technology, Seoul National University, Seoul 08826, Korea; Research Institute for Convergence Science, Seoul National University, Seoul 08826, Korea;* orcid.org/0000-0001-5745-313X; Email: kangwonlee@snu.ac.kr

Authors

Gyubok Lee − *Department of Applied Bioengineering, Graduate School of Convergence Science and Technology, Seoul National University, Seoul 08826, Korea;* orcid.org/0000-0001-6634-7523

Changheon Kim − *Program in Nanoscience and Technology, Graduate School of Convergence Science and Technology, Seoul National University, Seoul 08826, Korea;* orcid.org/0000-0002-5451-0853

Dongwoo Kim − *Department of Applied Bioengineering, Graduate School of Convergence Science and Technology, Seoul National University, Seoul 08826, Korea*

Changgi Hong − *Department of Applied Bioengineering, Graduate School of Convergence Science and Technology, Seoul National University, Seoul 08826, Korea*

Taeyong Kim − *Department of Materials Science and Engineering, College of Engineering, Seoul National University, Seoul 08826, Korea*

Moongoo Lee − *Department of Dentistry, School of Dentistry, Seoul National University, Seoul 08826, Korea*

Complete contact information is available at: https://pubs.acs.org/10.1021/acsomega.2c04129

https://doi.org/10.1021/acsomega.2c04129
ACS Omega XXXX, XXX, XXX−XXX

Author Contributions

G.L.: conceptualization, methodology, photographing, TOC graphic design, writing—original draft, writing—review and editing. C.K.: investigation, visualization, data analysis. D.K.: resources, formal analysis. C.H.: data curation, writing—review and editing. T.K.: software, validation, investigation. M.L.: investigation, software, validation. K.L.: supervision, funding acquisition, project administration.

Notes

The authors declare no competing financial interest.

■ ACKNOWLEDGMENTS

This research was supported by The Nano & Material Technology Development Program of the National Research Foundation of Korea (NRF) funded by the Ministry of Science and ICT (grant number: NRF2017M3A7B4049850). This work was in part supported by the Research Institute for Convergence Science.

■ REFERENCES

(1) Papatheodorou, K.; Banach, M.; Bekiari, E.; Rizzo, M.; Edmonds, M.Complications of Diabetes 2017. *J Diabetes Res***2018**, *2018*, 4. DOI: Artn 3086167 DOI: 10.1155/2018/3086167.

(2) Zhang, P.; Sun, D.; Cho, A.; Weon, S.; Lee, S.; Lee, J.; Han, J. W.; Kim, D. P.; Choi, W.Modified carbon nitride nanozyme as bifunctional glucose oxidase-peroxidase for metal-free bioinspired cascade photocatalysis. *Nat. Commun.***2019**, *10*, 940. DOI: ARTN 940 DOI: 10.1038/s41467-019-08731-y.

(3) Wang, T.; Tian, J.; Li, T. T.; Li, J.; Zhang, L. H. Enzyme properties and thermal stability of horseradish peroxidase (HRP-DL). *Aer Adv Eng Res* **2016**, *43*, 227−231.

(4) Sharifi, M.; Hosseinali, S. H.; Yousefvand, P.; Salihi, A.; Shekha, M. S.; Aziz, F. M.; JouyaTalaei, A.; Hasan, A.; Falahati, M. Gold nanozyme: Biosensing and therapeutic activities. *Mat Sci Eng C-Mater* **2020**, *108*, 110422 ARTN 110422.

(5) Jiang, Z. X.; Li, H.; Deng, Y. Q.; He, Y. Blue Light-Gated Reversible Silver Nanozyme Reaction Networks that Achieve Life-like Adaptivity. *Acs Sustain Chem Eng* **2020**, *8*, 5076−5081.

(6) Pedone, D.; Moglianetti, M.; Lettieri, M.; Marrazza, G.; Pompa, P. P. Platinum Nanozyme-Enabled Colorimetric Determination of Total Antioxidant Level in Saliva. *Anal. Chem.* **2020**, *92*, 8660−8664.

(7) Chang, M. Y.; Hou, Z. Y.; Wang, M.; Yang, C. Z.; Wang, R. F.; Li, F.; Liu, D. L.; Peng, T. L.; Li, C. X.; Lin, J. Single-Atom Pd Nanozyme for Ferroptosis-Boosted Mild-Temperature Photothermal Therapy. *Angew Chem Int Edit* **2021**, *60*, 12971−12979.

(8) Li, W. S.; Fan, G. C.; Gao, F. X.; Cui, Y. G.; Wang, W.; Luo, X. L. High-activity Fe3O4 nanozyme as signal amplifier: A simple, low-cost but efficient strategy for ultrasensitive photoelectrochemical immunoassay. *Biosens. Bioelectron.* **2019**, *127*, 64−71.

(9) Niu, X. H.; Xu, X. C.; Li, X.; Pan, J. M.; Qiu, F. X.; Zhao, H. L.; Lan, M. B. Surface charge engineering of nanosized CuS via acidic amino acid modification enables high peroxidase-mimicking activity at neutral pH for one-pot detection of glucose. *Chem. Commun.* **2018**, *54*, 13443−13446.

(10) Liu, W.; Tian, J. R.; Mao, C. L.; Wang, Z. F.; Liu, J.; Dahlgren, R. A.; Zhang, L. Z.; Wang, X. D. Sulfur vacancy promoted peroxidase-like activity of magnetic greigite (Fe3S4) for colorimetric detection of serum glucose. *Anal. Chim. Acta* **2020**, *1127*, 246−255.

(11) Nagvenkar, A. P.; Gedanken, A. Cu0.89Zn0.11O, A New Peroxidase-Mimicking Nanozyme with High Sensitivity for Glucose and Antioxidant Detection. *Acs Appl Mater Inter* **2016**, *8*, 22301−22308.

(12) Sun, H. J.; Zhou, Y.; Ren, J. S.; Qu, X. G. Carbon Nanozymes: Enzymatic Properties, Catalytic Mechanism, and Applications. *Angew Chem Int Edit* **2018**, *57*, 9224−9237.

(13) Jiang, D. W.; Ni, D. L.; Rosenkrans, Z. T.; Huang, P.; Yan, X. Y.; Cai, W. B. Nanozyme: new horizons for responsive biomedical applications. *Chem. Soc. Rev.* **2019**, *48*, 3683−3704.

(14) Tao, Y.; Ju, E. G.; Ren, J. S.; Qu, X. G. Bifunctionalized Mesoporous Silica-Supported Gold Nanoparticles: Intrinsic Oxidase and Peroxidase Catalytic Activities for Antibacterial Applications. *Adv. Mater.* **2015**, *27*, 1097−1104.

(15) He, W. W.; Zhou, Y. T.; Wamer, W. G.; Hu, X. N.; Wu, X. C.; Zheng, Z.; Boudreau, M. D.; Yin, J. J. Intrinsic catalytic activity of Au nanoparticles with respect to hydrogen peroxide decomposition and superoxide scavenging. *Biomaterials* **2013**, *34*, 765−773.

(16) Tseng, C. W.; Chang, H. Y.; Chang, J. Y.; Huang, C. C. Detection of mercury ions based on mercury-induced switching of enzyme-like activity of platinum/gold nanoparticles. *Nanoscale* **2012**, *4*, 6823−6830.

(17) Jv, Y.; Li, B. X.; Cao, R. Positively-charged gold nanoparticles as peroxidiase mimic and their application in hydrogen peroxide and glucose detection. *Chem. Commun.* **2010**, *46*, 8017−8019.

(18) Comotti, M.; Della Pina, C.; Matarrese, R.; Rossi, M. The catalytic activity of "Naked" gold particles. *Angew Chem Int Edit* **2004**, *43*, 5812−5815.

(19) Qian, K.; Sweeny, B. C.; Johnston-Peck, A. C.; Niu, W. X.; Graham, J. O.; DuChene, J. S.; Qiu, J. J.; Wang, Y. C.; Engelhard, M. H.; Su, D.; et al. Surface Plasmon-Driven Water Reduction: Gold Nanoparticle Size Matters. *J. Am. Chem. Soc.* **2014**, *136*, 9842−9845.

(20) Hafez, M. E.; Ma, H.; Ma, W.; Long, Y. T. Unveiling the Intrinsic Catalytic Activities of Single-Gold-Nanoparticle-Based Enzyme Mimetics. *Angew Chem Int Edit* **2019**, *58*, 6327−6332.

(21) Liu, S.; Tian, J. Q.; Wang, L.; Sun, X. P. Highly sensitive and selective colorimetric detection of Ag(I) ion using 3,3 ',5,5 ',-tetramethylbenzidine (TMB) as an indicator. *Sensor Actuat B-Chem* **2012**, *165*, 44−47.

(22) Yin, Z.; Wang, Y.; Song, C. Q.; Zheng, L. H.; Ma, N.; Liu, X.; Li, S. W.; Lin, L. L.; Li, M. Z.; Xu, Y.; et al. Hybrid Au-Ag Nanostructures for Enhanced Plasmon-Driven Catalytic Selective Hydrogenation through Visible Light Irradiation and Surface-Enhanced Raman Scattering. *J. Am. Chem. Soc.* **2018**, *140*, 864−867.

(23) Cheng, Z. Q.; Li, Z. W.; Yao, R.; Xiong, K. W.; Cheng, G. L.; Zhou, Y. H.; Luo, X.; Liu, Z. M.Improved SERS Performance and Catalytic Activity of Dendritic Au/Ag Bimetallic Nanostructures Based on Ag Dendrites. *Nanoscale Res. Lett.***2020**, *15*, 117. DOI: ARTN 117 DOI: 10.1186/s11671-020-03347-4.

(24) Piktel, E.; Suprewicz, L.; Depciuch, J.; Chmielewska, S.; Skłodowski, K.; Daniluk, T.; Król, G.; Kołat-Brodecka, P.; Bijak, P.; Pajor-Świerzy, A.; et al.Varied-shaped gold nanoparticles with nanogram killing efficiency as potential antimicrobial surface coatings for the medical devices. *Sci Rep-Uk***2021**, *11* (). DOI: ARTN 12546 DOI: 10.1038/s41598-021-91847-3.

(25) Li, J. R.; Zhang, G. N.; Wang, L. H.; Shen, A. G.; Hu, J. M. Simultaneous enzymatic and SERS properties of bifunctional chitosan-modified popcorn-like Au-Ag nanoparticles for high sensitive detection of melamine in milk powder. *Talanta* **2015**, *140*, 204−211.

(26) Wu, J. J. X.; Qin, K.; Yuan, D.; Tan, J.; Qin, L.; Zhang, X. J.; Wei, H. Rational Design of Au@Pt Multibranched Nanostructures as Bifunctional Nanozymes. *Acs Appl Mater Inter* **2018**, *10*, 12954−12959.

(27) Ma, T.; Yang, W. S.; Liu, S. M.; Zhang, H. J.; Liang, F.A Comparison Reduction of 4-Nitrophenol by Gold Nanospheres and Gold Nanostars. *Catalysts***2017**, *7* (). DOI: ARTN 38 DOI: 10.3390/catal7020038.

(28) Liu, M. Z.; Guyot-Sionnest, P. Synthesis and optical characterization of Au/Ag core/shell nanorods. *J. Phys. Chem. B* **2004**, *108*, 5882−5888.

(29) Zhou, X.; Liu, G. Q.; Zhang, H. W.; Li, Y.; Cai, W. P. Porous zeolite imidazole framework-wrapped urchin-like Au-Ag nanocrystals for SERS detection of trace hexachlorocyclohexane pesticides via efficient enrichment. *J. Hazard. Mater.* **2019**, *368*, 429−435.

(30) Li, J. R.; Lv, L.; Zhang, G. N.; Zhou, X. D.; Shen, A. G.; Hu, J. M. Core-shell Fructus Broussonetia-like Au@Ag@Pt nanoparticles as

https://doi.org/10.1021/acsomega.2c04129
ACS Omega XXXX, XXX, XXX−XXX

highly efficient peroxidase mimetics for supersensitive resonance-enhanced Raman sensing. *Anal Methods-Uk* **2016**, *8*, 2097−2105.
(31) Mohammad, F. A.; Al-Lohedan, H. N.; Al-Haque, H. Chitosan-mediated fabrication of metal nanocomposites for enhanced biomedical applications. *Advanced Materials Letters* **2017**, *8*, 89−100.
(32) Gabriel, E. F. M.; Garcia, P. T.; Cardoso, T. M. G.; Lopes, F. M.; Martins, F. T.; Coltro, W. K. T. Highly sensitive colorimetric detection of glucose and uric acid in biological fluids using chitosan-modified paper microfluidic devices. *Analyst* **2016**, *141*, 4749−4756.
(33) Jiang, C. F.; Zhu, J.; Li, Z.; Luo, J. H.; Wang, J. S.; Sun, Y. Chitosan-gold nanoparticles as peroxidase mimic and their application in glucose detection in serum. *Rsc Adv* **2017**, *7*, 44463−44469.
(34) Mohan, C. O.; Gunasekaran, S.; Ravishankar, C. N.Chitosan-capped gold nanoparticles for indicating temperature abuse in frozen stored products. *Npj Sci Food***2019**, *3* (). DOI: ARTN 2 DOI: 10.1038/s41538-019-0034-z.
(35) Cheng, L. C.; Huang, J. H.; Chen, H. M.; Lai, T. C.; Yang, K. Y.; Liu, R. S.; Hsiao, M.; Chen, C. H.; Her, L. J.; Tsai, D. P. Seedless, silver-induced synthesis of star-shaped gold/silver bimetallic nanoparticles as high efficiency photothermal therapy reagent. *J. Mater. Chem.* **2012**, *22*, 2244−2253.
(36) Zhang, X. Q.; Gong, S. W.; Zhang, Y.; Yang, T.; Wang, C. Y.; Gu, N. Prussian blue modified iron oxide magnetic nanoparticles and their high peroxidase-like activity. *J. Mater. Chem.* **2010**, *20*, 5110−5116.
(37) Cui, Y. S.; Lai, X.; Liang, B.; Liang, Y.; Sun, H. T.; Wang, L. G. Polyethyleneimine-Stabilized Platinum Nanoparticles as Peroxidase Mimic for Colorimetric Detection of Glucose. *Acs Omega* **2020**, *5*, 6800−6808.
(38) Geng, X.; Xie, X. N.; Liang, Y. C.; Li, Z. Q.; Yang, K.; Tao, J.; Zhang, H.; Wang, Z. Facile Fabrication of a Novel Copper Nanozyme for Efficient Dye Degradation. *Acs Omega* **2021**, *6*, 6284−6291.
(39) Gao, L. Z.; Zhuang, J.; Nie, L.; Zhang, J. B.; Zhang, Y.; Gu, N.; Wang, T. H.; Feng, J.; Yang, D. L.; Perrett, S.; et al. Intrinsic peroxidase-like activity of ferromagnetic nanoparticles. *Nat. Nanotechnol.* **2007**, *2*, 577−583.
(40) Zhang, L. N.; Deng, H. H.; Lin, F. L.; Xu, X. W.; Weng, S. H.; Liu, A. L.; Lin, X. H.; Xia, X. H.; Chen, W. In Situ Growth of Porous Platinum Nanoparticles on Graphene Oxide for Colorimetric Detection of Cancer Cells. *Anal. Chem.* **2014**, *86*, 2711−2718.
(41) Tian, R.; Sun, J. H.; Qi, Y. F.; Zhang, B. Y.; Guo, S. L.; Zhao, M. M.Influence of VO2 Nanoparticle Morphology on the Colorimetric Assay of H2O2 and Glucose. *Nanomaterials-Basel***2017**, *7* (). DOI: ARTN 347 DOI: 10.3390/nano7110347.
(42) Liu, Y. P.; Wang, C. W.; Cai, N.; Long, S. H.; Yu, F. Q. Negatively charged gold nanoparticles as an intrinsic peroxidase mimic and their applications in the oxidation of dopamine. *J. Mater. Sci.* **2014**, *49*, 7143−7150.

https://doi.org/10.1021/acsomega.2c04129
ACS Omega XXXX, XXX, XXX−XXX